# An Implementation of VFC for Stand-alone Asynchronous Generator Based Wind Energy Conversion System

S. Sharma [1] B. Singh [2]

**Abstract–This paper deals with an implementation of a VFC (Voltage and Frequency Controller) for a stand-alone WECS (Wind Energy Conversion System) based on an IAG (Isolated Asynchronous Generator) feeding 3-phase 4-wire loads. The proposed control scheme of VFC is based on SRF (Synchronous Reference Frame) theory for the estimation of reference source currents. The VFC consists of a 3-leg VSC (Voltage Source Converter) with a battery at its dc bus and a zig-zag/star transformer. Proposed VFC with bi-directional flow capability of active and reactive powers regulates the system voltage and frequency. The VFC is found capable to perform the functions of load leveling, harmonic elimination, voltage regulation and load balancing. The VFC is realized using a digital signal processor. Test results are presented to demonstrate the capabilities of proposed VFC for an IAG in the wind power generation.**

**Keywords–Asynchronous generator, voltage source converter, wind energy conversion system, zig-zag transformer**

## I. INTRODUCTION

From last few decades, there has been an extensive research on harnessing the potential of renewable energy sources especially wind, solar and tidal [1]. At present, the power crisis is severe in developing countries like India due to increase in the population and an enhanced use of electricity per capita. The situation is becoming rapidly worst due to depletion of fossil fuels. In some remote areas, the electricity through the grid connection is not feasible due to geo-graphic constraints. It is observed in such cases that, renewable energy sources may be viable option for power generation. In many applications such as off-shore petrochemical refining and water pumps in remote areas, grid-independent WECS (Wind Energy Conversion System) supported with the BESS (Battery Energy Storage System) may be suitable to supply electricity to isolated loads [2].

A capacitor excited asynchronous generator driven by a wind turbine has become quite popular in last decades due to its ruggedness, low maintenance and inherent short circuit protection capabilities [2]. Moreover it suffers from some fundamental problems like its inability to control the voltage under varying loads and prime-mover speed. To maintain constant voltage of IAG (Isolated Asynchronous Generator), a controlled reactive power support is mandatory [1-4]. When IAG is coupled with a wind turbine, an input power and the rotor speed both are varying depending on the wind speed, which leads to variation in the voltage and frequency [5-7].

Substantial work has been reported on the control of an IAG in an isolated wind power generation [8-9]. A stand-alone single phase induction generator is reported in the literature [8] in which the supply voltage and frequency are controlled by a single phase VSC (Voltage Source Converter) and a battery energy storage. In [9] simulation results are reported on VFC (Voltage and Frequency Controller) with a three-phase IAG, feeding three-phase four-wire consumer loads. However, very rare work is reported on its practical realization.

This paper deals with an implementation of VFC for an IAG based WECS using a DSP (Digital Signal Processor). A three leg VSC with a battery at its dc bus is used as a VFC. The zig-zag/star connected transformer is used in between VFC and the PCC (Point of Common Coupling). The SRF (Synchronous Reference Frame) theory [10] based current detection method is used to extract the fundamental active and reactive power components of the load currents. The unit templates $\sin\theta$ and $\cos\theta$ are estimated using phase voltages to obtain required transformation angle ($\theta$). The performance of VFC is demonstrated for the reactive power compensation to achieve constant terminal voltage, load leveling, harmonic compensation and load balancing with a BESS. In an isolated power generating system, harmonics compensation is also important because the supply voltage and current distortions adversely affect both consumers and IAG system.

## II. SYSTEM CONFIGURATION AND PRINCIPLE OF OPERATION

Fig. 1 shows a detailed block diagram of a proposed VFC for the WECS. It consists of a capacitor excited IAG to feed linear and non-linear consumer loads. A 3-leg VSC is used with a BESS as a VFC and it is connected at PCC through a zig-zag/star transformer. The VSC supplies the reactive power to IAG to regulate the voltage on application of different kinds of consumer loads. With the battery at its dc bus, an active power management takes place by exchanging the active power under varying input power and consumer loads. The battery absorbs the surplus power when the input wind power is more than the load demand and delivers the deficit power to common bus when the input wind power goes below the load demand. The frequency of the IAG depends directly on the availability of an input wind power and the load demand. The VSC consists of IGBTs (Insulated Gate Bipolar Transistors) based 3-leg module and a capacitor at its dc bus along with a BESS. Each leg consists of two IGBTs

The paper first received 9 Jun 2010 and in revised form 19 Jun 2013.
Digital Ref: APEJ-2013-04-417

[1] Electrical Engineering Department, Shri G. S. Institute of Technology & Science, Indore-452003, India email-ssharma.iitd@gmail.com
[2] Department of Electrical Engineering, Indian Institute of Technology Delhi, New Delhi-110016, India email-bsingh@ee.iitd.ac.in

and a common point of each leg is connected with an individual phase of the generator bus through an interfacing inductor and a zig-zag/star transformer. In practice, majority of small loads are single phase loads, therefore to take in to consideration, a three-phase four-wire system is developed in this WECS. The load neutral terminal is provided by the common terminal of the zigzag transformer. The proposed SRF control scheme is implemented using a DSP. The implementation of the VFC requires the proper selection of VSC, a BESS, an interface inductor, a scaling circuit for sensing the input signals and driver circuit for output signals.

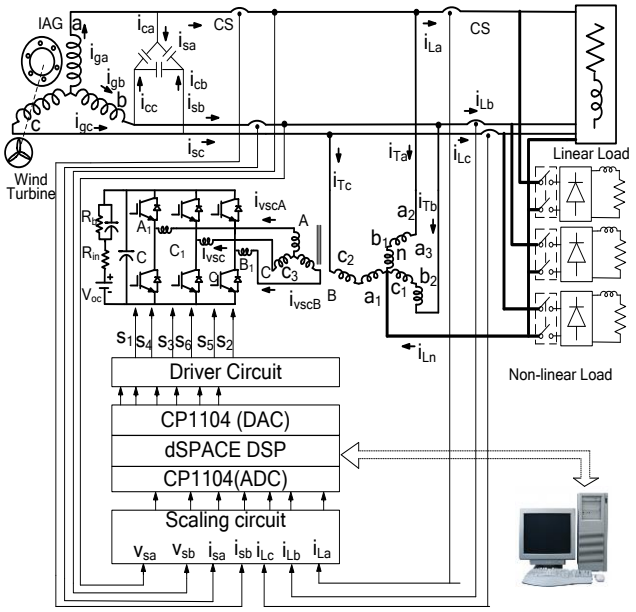


Fig. 1 System Configration of IAG based WECS

Three phase load currents are sensed using three Hall Effect current sensors (ABB EL50 BB). Another set of Hall Effect current sensors are used to sense two phase source currents. Since the generator is a star connected, therefore its third phase source current is estimated by considering that the algebraic sum of three phase source currents is zero. Two Hall Effect voltage sensors (LEM CV3-1500) are used to sense two phase voltages. Third phase voltage is estimated considering the algebraic sum of 3-phase source voltages is zero. A scaling circuit is used in between sensed signals and ADC of DSP to have a zero offset in the sensed signals. The control algorithm is realized in MATLAB environment in support with real time blocks. After compilation, program codes are loaded in the dSPACE DSP to generate the switching signals for IGBT's through DAC of DSP. An opto-coupler (6N136) based driver circuit is used to drive the IGBT module of VSC of VFC.

## III. Design of Voltage and Frequency Controller

The proposed VFC for a 3.7 kW, 230V IAG consists of a 3-leg CC-VSC (Current Controlled Voltage Source Converter) with a battery at its dc link (detailed data are given in Appendix). The mid-point of three half bridges are connected individually to each phase of IAG through an inductor. The zig-zag/star transformer is connected in between PCC and VSC. The zig-zag transformer provides a path for zero sequence components current present in the loads [11]. It consists of three single phase transformers with turn ratio of 1:1:1. For positive sequence and negative sequence currents, it behaves as an open circuit. The current flows in to it only when zero sequence currents present in load currents. The neutral terminal of the loads is connected with star terminal of a zig-zag transformer. In case of unbalanced loads, the zig-zag transformer provides the path for return load currents.

### *A. Design of Zig-zag/Star Transformer*

Fig. 2 shows a connection and phasor diagram of three single-phase transformers with three windings for each 1:1:1 turns-ratio as a zig-zag/star configuration. The zig-zag transformer provides a low impedance path for zero sequence currents, when connected in shunt at PCC [11]. The voltage across each winding of the transformer is 93 V for phase voltage of 132.79 V on primary winding side for 230V line voltage. The secondary windings are connected in star configuration and line voltage is 132.79 V.

Rating of a transformer depends on rating of an IAG and types of loads. Under no-load condition, the transformer has to feed full active power of an IAG to a BESS in addition to an exchange of reactive power from VSC needed for voltage control. Similarly under loading condition, the transformer has to exchange active and reactive powers through VSC for frequency and voltage control. Keeping under consideration all these aspects, three single-phase transformers of 1.5 kVA are selected with appropriate voltage and current ratings.

### *B. Excitation Capacitors*

An IAG needs the reactive power to build rated terminal voltage. The reactive power demand of an IAG is a function of consumer loads connected on the load bus. Therefore, the choice of an excitation capacitor affects VSC rating. In this case, the excitation capacitor is selected in such a way that it delivers rated voltage at 100% load on an IAG. A 4 kVAR delta connected capacitor bank is used in this implementation.

### *C. DC Bus Voltage*

The minimum dc bus voltage of VSC of VFC should be greater than twice the peak of phase voltage at the AC terminals of VSC [12]. The DC bus voltage is calculated as,

$$V_{dc} = \left(2\sqrt{2} / \sqrt{3}m\right)V_L \quad (1)$$

where m is the modulation index, considered 1 in this case and $V_L$ is the line rms voltage of secondary winding of the zig-zag/star transformer. Thus $V_{dc}$ is calculated as 217 V for $V_L$ (132 V) and it is selected as 240 V.

### *D. Selection of Battery*

Since a battery is an energy storage unit, its energy is in kWh (kilowatt-hours). As required $V_{dc}$ is more than 240V, therefore a minimum battery voltage is to be 240V. A battery with a capacity of 3.36 kWh is used for energy storage. For a DC bus voltage of 240 V, 20 units of 12 V,

7Ah are connected in series and two such strings are connected in parallel.

*E. AC Inductor*

The design of ac inductor depends on permissible current ripple ($i_{cr\_pp}$), DC bus voltage ($V_{dc}$) and switching frequency ($f_s$) of VSC and it is given as [12],

$$L_i = \frac{\sqrt{3} m V_{dc}}{12 a f_s i_{cr\_PP}} \quad (2)$$

where $m$ is a modulation index and $a$ is the overloading factor. Considering $m$=1, $V_{dc}$=240 V, $a$=1.2, $i_{cr\_pp}$=2 % and $f_s$=10 kHz, the value of $L_i$ is obtained as 1.44 mH. A round off value of 1.5 mH is selected in this investigation.

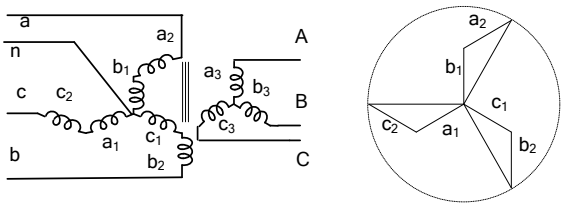


Fig. 2 Connection of a Zig-zag Transformer and its phasor diagram

## IV. CONTROL STRATEGY

As shown in Fig. 3, the control strategy of proposed VFC is realized using SRF theory for estimation of reference source currents. Load currents are sensed and transformed in to synchronous *d-q* rotating frame and required transformation angle ($\theta$) is achieved using in-phase (sin$\theta$) and quadrature (cos$\theta$) templates for phase 'a' over PCC voltages. The *q*-axis component of reference source currents is estimated as a difference of an output of a voltage PI (Proportional-Integral) controller and output of filtered *q*-axis component of load currents. The *d*-axis component of reference source currents is estimated as a difference of output of frequency PI controller and output of filtered *d*-axis component of load currents.

Basic equations of the control algorithm used in proposed VFC are as follows.

*A. Estimation of Transformation Angle and IAG Frequency*

The transformation angle ($\theta$) is required for SRF theory. In this implementation, it is obtained using in-phase and quadrature templates. The in-phase unit templates are derived using amplitude of PCC voltage, $V_t$ and phase voltages as,

$$V_t = \sqrt{2(v_a^2 + v_b^2 + v_c^2)/3} \quad (3)$$

$$u_{ap} = v_a / V_t, u_{bp} = v_b / V_t, u_{cp} = v_c / V_t \quad (4)$$

Moreover, quadrature unit template for phase 'a' is as,

$$u_{aq} = (-u_{bp} + u_{cp}) / \sqrt{3} \quad (5)$$

The in-phase unit templates are in phase with the IAG terminal voltages, so it can be considered as a sinusoidal function rotating at an angular frequency of an IAG voltage. The quadrature unit template of phase 'a' is shifted from in-phase unit template by an angle of $90^0$, so it can be treated as a cosine function rotating with an IAG angular frequency.

$sin\theta = u_{ap}$,

$cos\theta = u_{aq}$ (6)

The instantaneous value of '*f*' is estimated using in-phase and quadrature templates for phase 'a'. The supply frequency $w_{ms}$ in radian/sec can be expressed as,

$$w_{ms} = \cos\theta\, p(\sin\theta) - \sin\theta\, p(\cos\theta) \quad (7)$$

where $p$ is the time derivative operator and IAG frequency is as $f = w_{ms}/(2\pi)$.

*B. Synchronous Reference Frame Theory*

In the SRF, the load currents are transformed into the synchronous rotating frame *d-q* current components. If θ is the transformation angle, the transformation is defined as,

$$\begin{bmatrix} i_{Ld} \\ i_{Lq} \\ i_0 \end{bmatrix} = \sqrt{\frac{2}{3}} \begin{bmatrix} \cos(\theta) & \cos(\theta - 2\pi/3) & \cos(\theta + 2\pi/3) \\ \sin(\theta) & \sin(\theta - 2\pi/3) & \sin(\theta + 2\pi/3) \\ 1/\sqrt{2} & 1/\sqrt{2} & 1/\sqrt{2} \end{bmatrix} \begin{bmatrix} i_{La} \\ i_{Lb} \\ i_{Lc} \end{bmatrix} \quad (8)$$

where $i_{Ld}$, $i_{Lq}$ and $i_0$ denote load currents in *d-q* reference frame and $i_{La}$, $i_{Lb}$ and $i_{Lc}$ are sensed three-phase load currents. In SRF, $\theta$ is a time varying angle that represents an angular position of the reference frame, rotating at constant speed in synchronism with a phase 'a' voltage. (8) transforms fundamental currents in *abc* axis to dc values in *d-q* reference frame. Harmonics appear like ripples. It is desired that IAG should have only fundamental component of *d-q* axes currents required for the system. Harmonics present in load currents are supplied by a VSC. A low pass Butter-worth filter is used with a cut-off frequency of 25 Hz to extract dc components from *d-q* axes load currents ($i_{Lddc}$, $i_{Lqdc}$) as shown in Fig. 3.

*C. Direct Axis Component of Reference Source Currents*

Direct axis component of reference source current is estimated by a difference of a dc component of d-axis load current ($i_{Ldc}$) and an output of frequency PI (Proportional-Integral) controller ($i_{fd}$). The frequency error is defined as,

$$f_e(n) = f_{rf}(n) - f\,(n) \quad (9)$$

where '$f_{rf}$' is the reference frequency ( i.e. 50 Hz in this case) and '*f*' is the frequency of the terminal voltage of an IAG as estimated using (7).

At the $n^{th}$ sampling instant, the output of the frequency PI controller ($i_{fd}$) is as,

$$i_{fd}(n) = i_{fd}(n-1) + k_{pf}\{f_e(n) - f_e(n-1)\} + k_{if}\, f_e(n) \quad (10)$$

Therefore, the instantaneous value of direct axis component of reference source currents ($i^*_{sd}$) is as,

$$i^*_{sd} = i_{fd} - i_{Lddc} \quad (11)$$

*D. Quadrature Axis Component of Reference Source Currents*

The difference of an output of voltage PI controller and the filtered *q*-axis load currents is used to generate the quadrature axis reference source current. The ac voltage error at the $n^{th}$ sampling instant is as,

$$V_e(n) = V_{tr}(n) - V_t(n) \tag{12}$$

where $V_{tr}(n)$ is the amplitude of the reference ac terminalphase voltage and $V_t(n)$ is the amplitude of sensed three phase ac voltages at PCC at the $n^{th}$ sampling instant. The amplitude of $V_t$ is estimated using (3) and the output of voltage PI controller for maintaining a constant ac terminal voltage at the $n^{th}$ sampling instant is expressed as,

$$i_{vq}(n) = i_{vq}(n-1) + k_{pa}\{V_e(n) - V_e(n-1)\} + k_{pi}V_e(n) \tag{13}$$

where $k_{pa}$ and $k_{ia}$ are the proportional and integral gain constants of the PI controller. $V_e(n)$ and $V_e(n-1)$ are the voltage errors in the $n^{th}$ and $(n-1)^{th}$ sampling instant. The $i_{vq}(n)$ and $i_{vq}(n-1)$ are the amplitude of output of voltage PI controller in the $n^{th}$ and $(n-1)^{th}$ instant needed for voltage control.

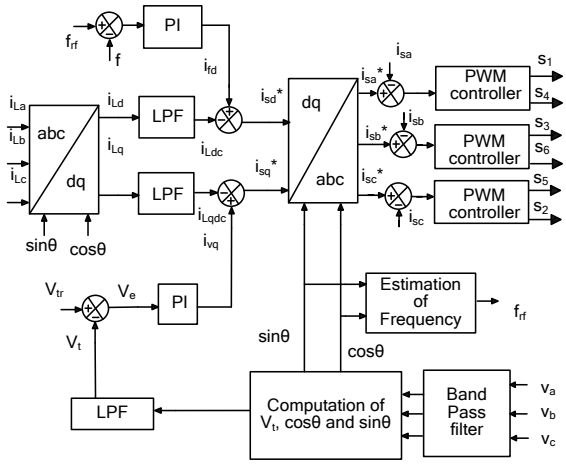


Fig. 3 Control Shceme of the proposed Controller

Quadrature axis component of reference source currents is as,

$$i^*_{sq}(n) = i_{vq}(n) - i_{Lqdc}(n) \tag{14}$$

*E. Three Phase Reference Source Currents*

The reference direct axis and quadrature axis source currents are transformed into three phase source currents using inverse Park's transformation as,

$$\begin{bmatrix} i^*_{sa} \\ i^*_{sb} \\ i^*_{sc} \end{bmatrix} = \sqrt{\frac{2}{3}} \begin{bmatrix} \sin(\theta) & \cos(\theta) & 1/\sqrt{2} \\ \sin(\theta - 2\pi/3) & \cos(\theta - 2\pi/3) & 1/\sqrt{2} \\ \sin(\theta + 2\pi/3) & \cos(\theta + 2\pi/3) & 1/\sqrt{2} \end{bmatrix} \begin{bmatrix} i^*_{sd} \\ i^*_{sq} \\ i^*_{s0} \end{bmatrix} \tag{15}$$

where $i^*_{s0}$ is zero for proposed IAG system.

*F. Current Controller*

These three-phase reference source currents ($i^*_{sa}$, $i^*_{sb}$, $i^*_{sc}$) are compared with sensed source currents ($i_{sa}$, $i_{sb}$, $i_{sc}$). The independent carrier-less PWM controllers are used for each leg of VSC. When the current error for individual phase exceeds upper band, the lower switch is switched on and the upper switch is off and when the current error falls below the lower band, an upper switch is switched on keeping the lower switch off. The current tolerance band 0.2A is selected in this implementation.

## V. Results And Discussion

The developed VFC is tested with non-linear loads. Load perturbations with non-linear loads are made and results are recorded in terms of the generator line voltage ($v_{ab}$), generator currents ($i_{ga}$, $i_{gb}$ and $i_{gc}$), source currents ($i_{sa}$, $i_{sb}$ and $i_{sc}$), capacitor currents ($i_{ca}$, $i_{cb}$ and $i_{cc}$), zig-zag/star transformer primary winding currents ($i_{Ta}$, $i_{Tb}$ and $i_{Tc}$), VSC currents ($i_{vscA}$, $i_{vscB}$ and $i_{vscC}$) and battery current ($I_b$).

*A. Performance of the VFC with Non-linear Loads*

Performance of the VFC is demonstrated with non-linear loads. A diode bridge rectifier with resistive-inductive load is chosen as a non-linear load to study the operation of the VFC as a voltage regulator, harmonics eliminator and as a load leveler. The steady state performance of the controller is shown in Fig. 4. Test results are recorded with $v_{ab}$. The $i_{ga}$, $i_{gb}$ and $i_{gc}$ are shown with $v_{ab}$ in Figs. 4 (a-c). The $i_{ca}$, $i_{cb}$ and $i_{cc}$ along with $v_{ab}$ are given in Figs. 4 (d-f). Source currents, $i_{sa}$, $i_{sb}$ and $i_{sc}$ and load currents $i_{La}$, $i_{Lb}$ and $i_{Lc}$ are recorded with $v_{ab}$ and shown in Figs. 4 (g-l). Transformer primary winding currents $i_{Ta}$, $i_{Tb}$ and $i_{Tc}$ with $v_{ab}$ are shown in Figs. 5 (a-c). The generator is loaded with almost its rating during this case and $P_g$, $P_L$ and $P_b$ are shown in Figs. 5 (d-f). The recorded harmonic spectra of generator voltage, generator current, and load current are shown in Figs. 5 (g-i). THD's of generator current and voltage are well within IEEE- 519 limits.

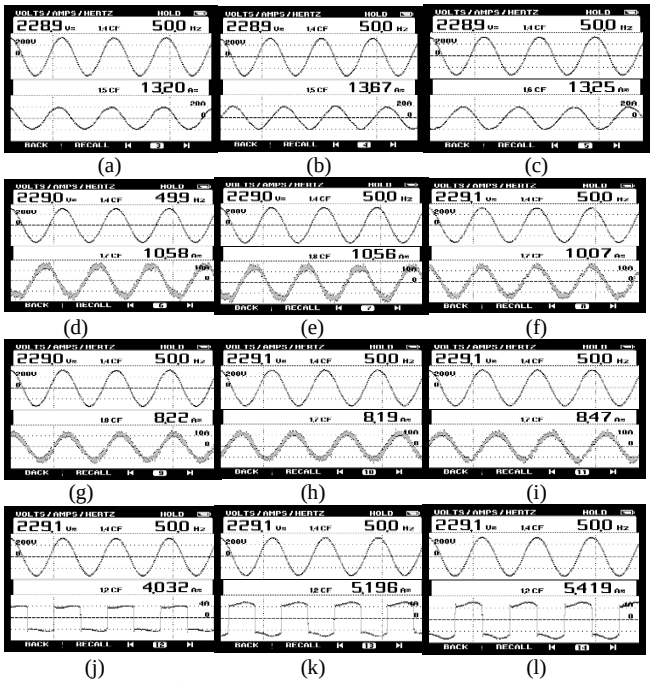


Fig. 4 Test results of WECS (a) $v_{ab}$ and $i_{ga}$ (b) $v_{ab}$ and $i_{gb}$ (c) $v_{ab}$ and $i_{gc}$ (d) $v_{ab}$ and $i_{ca}$ (e) $v_{ab}$ and $i_{cb}$ (f) $v_{ab}$ and $i_{cc}$ (g) $v_{ab}$ and $i_{sa}$ (h) $v_{ab}$ and $i_{sb}$ (i) $v_{ab}$ and $i_{sc}$ (j) $v_{ab}$ and $i_{La}$ (k) $v_{ab}$ and $i_{Lb}$ (l) $v_{ab}$ and $i_{Lc}$

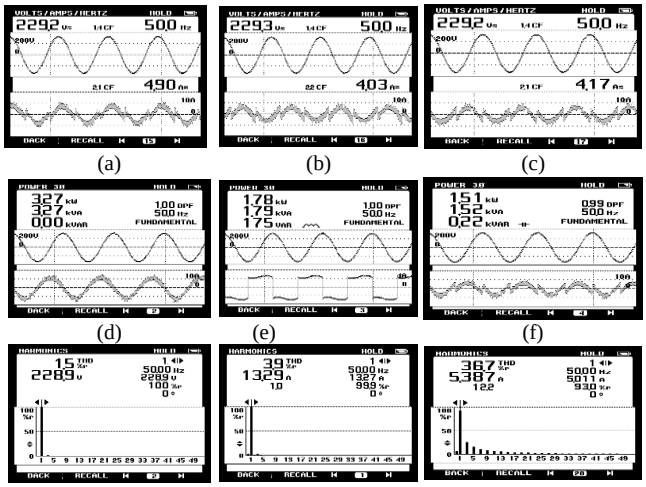

(a) (b) (c)

(d) (e) (f)

(g) (h) (i)

Fig. 5 Test results of WECS (a) $v_{ab}$ and $i_{Ta}$ (b) $v_{ab}$ and $i_{Tb}$ (c) $v_{ab}$ and $i_{Tc}$ (d) $v_{ab,}$ $i_{sc}$ and $P_g$ *(e)* $v_{ab,}$ $i_{Lc}$ and $P_L$ *(f)* $v_{ab,}$ $i_{Tc}$ and $P_b$ *(g)* harmonic spectrum of $v_{ab}$ *(h)* harmonic spectrum of $i_{gc}$ *(i)* harmonic spectrum of $i_{Lc}$

### *B. Performance of the VFC during Load Removal*

Fig. 6 shows the dynamic performance of the VFC at the load removal on one phase. Test results are recorded using Agilent make digital oscilloscope (DSO6014A), voltage differential probe (1/100), current probe (100mA/V). The waveforms of various quantities are recorded with $v_{ab}$. Figs. 6 (a) show the change in $P_g$, $P_b$ and $P_L$ during removal of the load on phase 'b'. The $P_g$ remains almost constant and reduction in load power results in increased charging of BESS with difference of $P_g$ and $P_L$. Fig. 6 (b) shows the load currents $i_{La}$, $i_{Lb}$ and $i_{Lc}$ at removal of load on phase 'b'. The variation in transformer currents $i_{Ta}$, $i_{Tb}$ and $i_{Tc}$ are observed in Fig. 6(c). It is clearly seen that during the load removal on phase 'b' leads to necessary change in $i_{Tb}$ magnitude. The VSC currents $i_{vscA}$, $i_{vscB}$ and $i_{vscC}$ are shown in Fig. 6 (d) and are in agreement with recorded results shown in Fig. 6 (c). Source currents are shown in Fig. 6 (e) at load removal on phase 'b' and almost steady state during load perturbation and agree with the results shown in Fig. 6 (a). The change in battery current ($I_B$) and source current ($i_{sb}$) are recorded with $i_{Lb}$ during dynamic conditions and are shown in Fig. 6 (f).

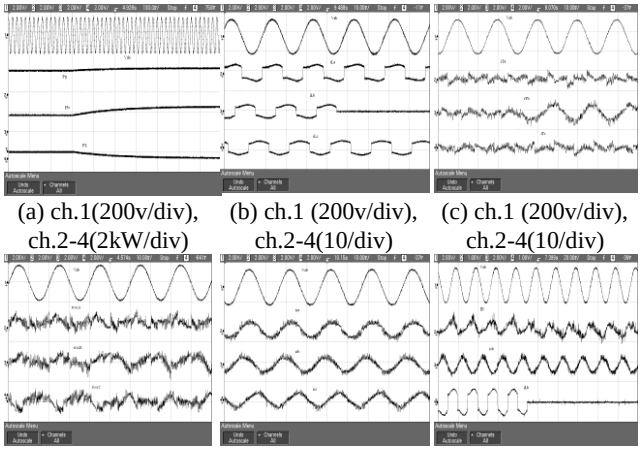

(a) ch.1(200v/div), ch.2-4(2kW/div) (b) ch.1 (200v/div), ch.2-4(10/div) (c) ch.1 (200v/div), ch.2-4(10/div)

(d) ch.1 (200v/div), ch.2-4(10/div) (e) ch.1 (200v/div), , ch.2-4(10/div) (f) ch.1 (200v/div), ch.2-4(10/div)

Fig. 6 Test results of WECS, dynamics at load removal (a) $v_{ab,}$ $P_g$, $P_L$ and $P_b$ (b) $v_{ab,}$ $i_{La}$, $i_{Lb}$ and $i_{Lc}$ (c) $v_{ab,}$ $i_{Ta}$, $i_{Tb}$ and $i_{Tc}$ (d) $v_{ab,}$ $i_{vscA}$, $i_{vscB}$ and $i_{vscC}$ (d) $v_{ab}$ ,$I_b$, $i_{sb}$ and $i_{Lb}$ (e) $v_{ab,}$ $i_{sa}$, $i_{sb}$ and $i_{sc}$

### *C. Performance of the VFC at Load Application*

Fig. 7 shows the dynamic performance of VFC at load application. Fig. 7 (a) shows the change in $P_g$, $P_b$ and $P_L$ at the load application on phase 'b'. $P_g$ remains almost constant and a rise is observed in $P_L$ while decrease in $P_b$ is recorded. Fig. 7 (b) shows load currents $i_{La}$, $i_{Lb}$ and $i_{Lc}$ during the application of the load on phase 'b' which leads to balanced load currents. The variation in $i_{Ta}$, $i_{Tb}$ and $i_{Tc}$ are shown in Fig. 7(c). It is clearly seen that applying load on phase 'b' leads to necessary reduction in $i_{Tb}$ magnitude and after load application $i_{Ta}$, $i_{Tb}$ and $i_{Tc}$ magnitude are observed identical. VSC currents $i_{vscA}$, $i_{vscB}$ and $i_{vscC}$ are shown in Fig. 7(d). Source currents are shown in Fig. 7 (e) at load application on phase 'b' and these remain almost steady-state during sudden change in loads. The change in $I_b$ and $i_{sb}$ are recorded with $i_{Lb}$ under dynamic conditions and are shown in Fig. 7 (f).

### *D. Dynamic Performance of the VFC*

The wind power and consumer loads connected with the WECS both vary in practice. Therefore it is required to verify the performance of VFC under both these conditions. Test results shown in Figs. 6 and 7 have verified capabilities of VFC under dynamic conditions. Fig. 8(a) shows the variations in important parameters of WECS, while keeping the load power constant. In the case when the generated power ($P_g$) is more than the consumer load demand ($P_L$), the battery ($P_b$) absorbs the surplus power. The battery supplies the deficit load power when the generated power is less than the load demand. Fig. 8(b) shows the variations in battery power ($P_b$) and battery charging current ($I_b$) under change in consumer load demand ($P_L$) while keeping the generated power ($P_g$) constant. As the $P_L$ increases, there is a reduction in $P_b$ and $I_b$ and when the $P_L$ exceeds the $P_g$, the battery starts supplying the deficit power, therefore $P_{b,}$ and $I_b$ are observed negative.

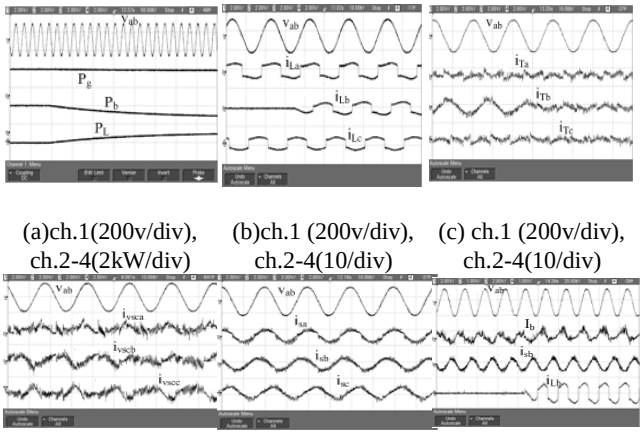

(a)ch.1(200v/div), ch.2-4(2kW/div) (b)ch.1 (200v/div), ch.2-4(10/div) (c) ch.1 (200v/div), ch.2-4(10/div)

(d)ch.1(200v/div), ch.2-4(10/div) (e)ch.1 (200v/div), ch.2-4(10/div) (f)ch.1 (200v/div), ch.2-4(10/div)

Fig. 7 Test results of WECS, dynamics with load application (a) $v_{ab,}$ $P_g$, $P_L$ and $P_b$ (b) $v_{ab,}$ $i_{La}$, $i_{Lb}$ and $i_{Lc}$ (c) $v_{ab,}$ $i_{Ta}$, $i_{Tb}$ and $i_{Tc}$ (d) $v_{ab,}$ $i_{vscA}$, $i_{vscB}$ and $i_{vscC}$ (d) $v_{ab}$ ,$I_b$, $i_{sb}$ and $i_{Lb}$ (e) $v_{ab,}$ $i_{sa}$, $i_{sb}$ and $i_{sc}$

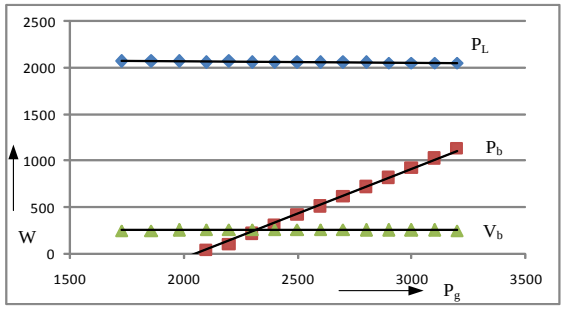


(a)

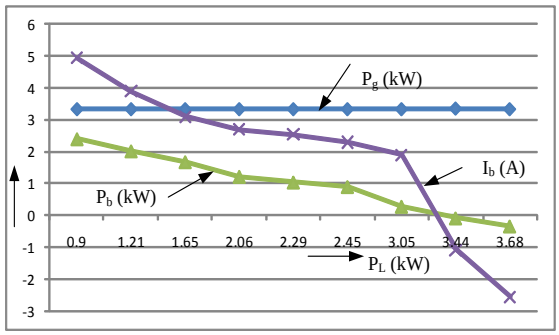


(b)

Fig. 8 (a) Load power ($P_L$), battery power ($P_b$), battery voltage ($V_b$) under variations in generated power ($P_g$), (b) Generated power ($P_g$), battery power ($P_b$) and battery current ($I_b$) under variation in load power ($P_L$)

## VI. Conclusion

A prototype of VFC has been implemented for the IAG based stand-alone WECS. Test results have verified the control algorithm and it has performed well under both steady state and dynamic conditions. The battery supported VFC has provided the load leveling, load balancing, neutral current compensation and harmonic elimination along with voltage and frequency control.

## Appendix

| | |
|---|---|
| IAG Data | 3.7 kW, 230 V, 14.5 A, 50 Hz, Y-Connected, 4-Pole |
| Prime-Mover Data | 3.7 kW, 415 V, 7A, Δ-connected, 4-pole, 1430 rpm, induction motor driven by ABB make AC Drive ACS 550-01-015A |
| VFC Parameters | Semikron make voltage source converter 25kVA, $L_f$=1.5 mH, $R_f$= 0.01 Ω, $C_{dc}$=4000 μF, $K_{pav}$=0.1, $K_{aiv}$=0.01, $K_{paf}$=5, $K_{pif}$=.54 |
| Battery Rack | $V_{dc}$=240V, 3.36kWh, Each rack has 20 units of 12 V, 7Ah connected in series and two such racks are used |
| zig-zag/ Star Transformer | 4.5kVA, 3-phase transformer with each phase having three windings with 139V ratings |

## References

[1] M.G. Simos and F. A. Ferret, Renewable Energy systems. Orlando, Fl: CRC, 2004.

[2] Ion Boldea, Variable Speed Generator, The Electrical Generator Handbook, New York: Taylor & Francis, CRC, 2006.

[3] G. Raina and O.P. Malik, "Wind Power Conversion using a Self Excited Induction Generator", *IEEE Trans. on Power App. and Syst.*, vol. PAS-102, no.12, pp. 3933-3936, Dec.1983.

[4] J. Faiz, "Design and implementation of a solid state controller for regulation of output voltage of a wind driven self-excited three phase squirrel cage induction generator", in Proc. *IEEE 8th Int. Conf. Elect. Mech. Syst.*, vol.3, pp. 2384-2388, Sep.2005.

[5] C.V Nayar and J.H. Bundell, "Output Power Controller for a Wind-Driven Induction Generator", *IEEE Trans. on Aerosp. and Electron. Syst,*, vol. AES-23, no. 3, pp. 388 – 401, May 1987.

[6] Q. Wang and L. Chang, "An Intelligent maximum Power Extraction Algorithm for Inverter-Based Variable Speed Wind Turbine Systems", *IEEE Trans. Power Electron*., vol. 19, no.5, pp. 1422-1429, Sept.2004.

[7] S.S. Murthy, B. Singh, S. Gupta and B.M. Gulati, "General steady-state analysis of three-phase self-excited induction generator feeding three-phase unbalanced load/single-phase load for stand-alone applications", *IEE Proc. Gen., Trans. & Distrib.* vol.150, no.1, pp.49–55, Jan. 2003.

[8] O. Ojo, O. Omozusi, A. Ginart and B. Gonoh, "The Operation of Stand-Alone Single-phase Induction Geneerator using a Single-Phase Pulse-Width modulated Inverter With a Battery Supply", *IEEE Trans. on Energy Conver.*, vol. 14, no. 3, pp. 526-531, Sept.1999.

[9] B. Singh and G. Kasal, "Voltage and Frequency Controller for a Three Phase Four –Wire Autonomous Wind Energy Conversion System*", IEEE Trans. on Energy Conver.*, vol. 23, no. 2, pp. 509-518, June 2008.

[10] Bhim Singh, P Jayaprakash and D P Kothari, "A T-Connected Transformer and Three-Leg VSC Based DSTATCOM for Power Quality Improvement", *IEEE Trans. Power Electron*., vol. 23, no. 6, pp. 2710 -2718, November 2008.

[11] H-L Jou, K-Der Wu, Jinn-Chang Wu and Wen-Jung Chaing, "A Three- Phase Four-Wire Filter Comprising a Three-Phase Three- Wire Active Power Filter and a Zig-Zag Transfromer", *IEEE Trans. Power Electron*., vol. 23, no. 1, pp. 252-259, Jan. 2008.

[12] B. N. Singh, P. Rastgoufard, B. Singh, A. Chandra, and K. Al. Haddad, "Design, simulation and implementation of three pole/four pole topologies for active filters", *Inst. Electr. Eng. Proc. Electr. Power Appl.*, vol. 151, no. 4, pp. 467–476, Jul. 2004.

## Biographies

**Shailendra Sharma** was born in Indore, India, in 1972. He received M.E. in Electrical Engineering with specialization in power electronics in 2004 from Shri G. S. Institute of Technology & Science, Indore, India and Ph.D. degree from the Indian Institute of Technology Delhi, New Delhi, India in 2012. He has an industrial experience of five years as a erection & commissioning engineer with M/s Dhar Textile Mills Ltd, Indore, India. He joined the Department of Electrical Engineering, Shri GSITS, Indore in 2004 as a lecturer. His fields of interest are power electronics, Drives, power quality, and renewable energy. He is a Memebr of IEEE and Associate Member of the Institution of Engineers India.

**Bhim Singh** was born in Rahamapur, India, in 1956. He received the B.E (Electrical) degree from the University of Roorkee, Roorkee, India, in 1977 and the M.Tech and Ph.D. degree from the Indian Institute of Technology (IIT) Delhi, New Delhi, India, in 1979 and 1983, respectively. In 1983, he joined the Department of Electrical Engineering, University of Roorkee, as a Lecturer, and in 1988 became a Reader. In December 1990, he joined the

Department of Electrical Engineering, IIT Delhi, as an Assistant Professor. He became an Associate Professor in 1994 and Professor in 1997. His area of interest includes power electronics, electrical machines and drives, active filters, FACTS, HVDC and power quality. He is a fellow of Indian National Academy of Engineering (INAE), National Science Academy (FNSc), the Institution of Engineers (India) (FIE(I)), and the Institution of Electronics and Telecommunication Engineers (FIETE), a life member of the Indian Society for Technical Education (ISTE), the System Society of India (SSI), and the National Institution of Quality and Reliability (NIQR), Fellow of IET and Fellow of Institute of Electrical and Electronics Engineers (FIEEE).